# Efficient CFD methods for assessment of water management

Martin Novák[1], Rene Devaradja[1], Jacques Papper[1] and Martin Černý[2]

[1] Icon Technology & Process Consulting Ltd.
[2] ŠKODA AUTO a.s.

**Abstract.** An unobscured view from the vehicle during rainy weather conditions is essential for occupants' safety and comfort. With the decrease in the time available for vehicle development and testing, it is becoming even more important to control and predict vehicle water management early in the development cycle to avoid undesired soiling effects. To do so, a transient external aerodynamics airflow coupled with a discrete particle phase is simulated, where rain droplets away from the vehicle are modeled as Lagrangian particles and rain droplets that impact the vehicle are represented through a film model. A novel, time-efficient implementation of a windscreen wiper based on [1] within iconCFD [2] is also summarized. A representative example - rain-induced reduced visibility on the side window - is considered to discuss the physics, time scales, and recommended best practices for rain soiling simulations. The simulation results for this example case are compared with experimental data.

**Keywords:** CFD validation, exterior water management, A-pillar overflow, wiper, film.

## 1 Introduction

Exterior Water Management (EWM) has always been an important aspect of vehicle functional external aerodynamics. The ability of the car shape to minimize the amount of water deposited and stagnating in areas that affect the driver's line of sight is a crucial aspect of a given vehicle's functional safety. As the time of prototyping and vehicle development decreases and the amount of physical hardware testing reduces, it is crucial to substitute those tests virtually and introduce them early into the design process [3].

This is even more critical with the recent ever-increasing demand for optimized aerodynamics. Some of the requirements for minimizing drag and wind noise around the A-pillar and side mirror conflict with the needs of robust and safe water management. Indeed, these requirements directly affect the front side window visibility and the cleanliness of the glass of the side mirrors. Traditional EWM features, such as channels or gutters along the inboard edges of the A-pillar and specific sizes and shapes of the side mirrors, are recently being revisited to avoid the issues mentioned previously and to thereby further improve the vehicle's performance and comfort.

Any viable virtual method that aims to evaluate an A-pillar design needs to be sufficiently refined so it can predict both the influence of traditional geometrical feature modifications and also the effect of a novel, more subtle, means of EWM, such as hydrophobic surface finishes. At the same time, the virtual method needs to be robust enough to cope with high water levels due to the action of the wipers and rapid enough to produce results that can be compared and balanced against the outcomes of the early development of external aerodynamics and aeroacoustics.

Achieving all of the above is the goal of the presented methodology. In this article, after a brief introduction, the goals of the EWM relevant to side-window visibility are summarized and the *Experimental methods* needed for rigorous correlation and validation of the presented CFD analysis are outlined. A brief review of available methods is presented in section *Modeling: State of the Art*, which also provides the context regarding the used methods. The general features of the methods used are placed in the *Virtual Representation section*. This virtual model is applied and correlated against experimental data provided by SKODA AUTO. This article does not aim to evaluate the production vehicle design; rather its goal is to present given features of the applied methodology and to show how they can be used to guide the development of robust EWM with regards to front side window visibility utilizing a Continuous Phase Film Model (CPFM) and a new IBM based model of windscreen wiper implemented in iconCFD.

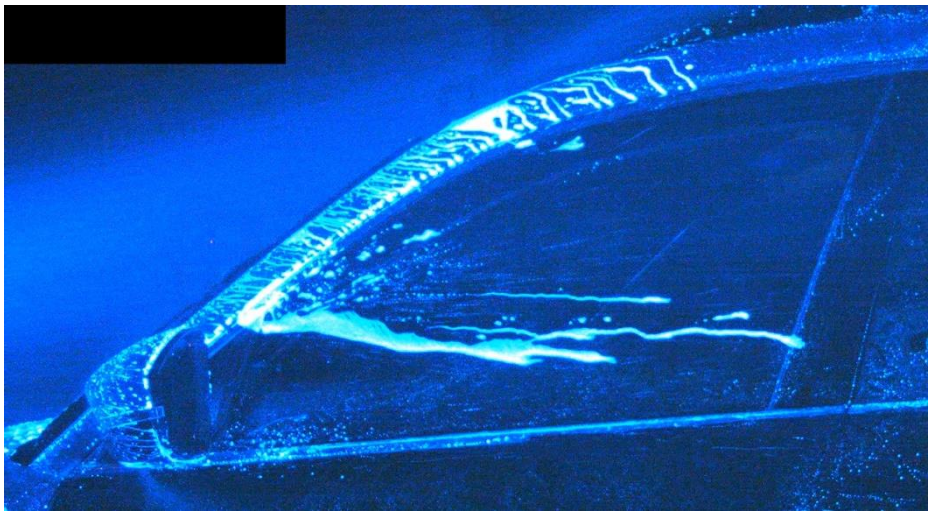

**Fig. 1.** Illustration of a common water pattern on a side window.

## 2 Exterior Water Management

As stated in [3], EWM involves the following physics:

1. The multiphase flow (rain, air and droplets) in front of and around the geometry with all its complexity (e.g. turbulence, phase coupling, properties of the dispersed phase, etc.).

2. Spray-wall interactions.
3. The build-up of a liquid film on a surface.
4. The development of a liquid film along a surface, including instability considerations.
5. Film break-up.
6. The re-entrainment of separated liquid regions (secondary droplets) by the airflow, possibly leading to further droplet impacts

Historically, the major focus has been related to reduced visibility due to water film deposition and motion on windows. The issue on the front windshield can be resolved by a suitable windscreen wiper. However, this only shifts the water management issue elsewhere, since the excess water removed by the wiper blade is moved toward the A-pillar that links the front windshield with the front-side glass. Here, the overflow of the A-pillar can cause a safety-related issue with reduced visibility of the side rear view mirror (as illustrated in Figure 1.). To avoid this, the A-pillar is designed with intricate water management features such as steps or channels. However, those features have to be subtle so that they do not compromise the aerodynamic performance of the vehicle shape. Also, the visibility through the front-side window is further impaired by the interaction of rain with the side mirror and the side-mirror wake. This wake can deposit water on the side window either from the rain or even from water stripped from the mirror itself [4].

In the presented article, tasks 1-4 are studied whereas 5-6 are neglected.

## 3 Experimental Set-up

To replicate on-road conditions, significant progress has been made over the past years in the field of wind tunnel testing to allow for experiments that give both qualitative ( [4], [5]) and recently also quantitative [6] observations about the soiling of the side window. Usually, an experimental setup in a climatic wind tunnel consists of a spray rack that emits water droplets at a defined volume flow rate, while the wind tunnel blows air with a defined speed and temperature. For the test setup related to front-side window visibility, a spray rack with water spray nozzles is placed in the wind tunnel nozzle in front of the stationary vehicle in the test section (schematics in Figure 2). Unlike the case of self-soiling, the wheels rotation and floor movement are of negligible influence and are kept stationary. The car surface is cleaned with a water jet and dried so the surface is not prewetted. The wind tunnel is set to the test airspeed, the wipers are turned on and the injection is started.

To visualize the water and to gain insight into its behavior, a UV-tracer fluid is added to the fluid. This forms a solution that is possible to trace with UV-cameras due to illumination from UV-lights that are on during the test. In the simulation, the material properties of the mixture are assumed to be identical to water at a given temperature.

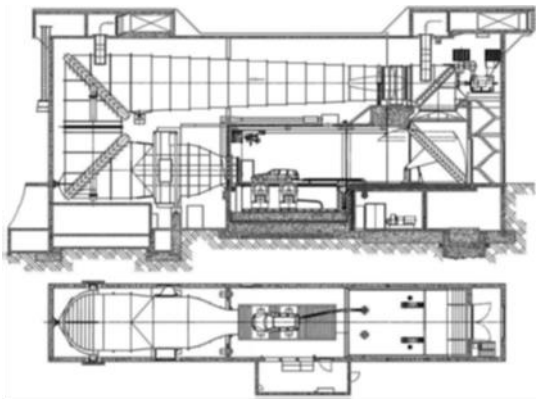

**Fig. 2.** The schematics of the FKFS thermal wind tunnel [7], side view (top) and top view (bottom)

## 4 Modeling: State of the Art

The current state of 3D CFD simulations of vehicle water management still follows the three-step approach initially introduced by Karbon and Longman [8] and Foucart [9]:

- Compute 3D airflow that is representative of the studied simulation, often by employing the existing numerical external aerodynamics methodology
- Introduce the droplets representing the rain into the flow domain and conduct a transient simulation that tracks their motion to predict the location and speed with which they impact the body panels or windows
- Resolve the water flow that is deposited on the vehicle body from the rain

An extensive review of the methods and practices in vehicle soiling and water management is given in [3] and more recently in [10]. In the case of an A-pillar overflow, a method to first identify the breaching point on an A-pillar [11] has been developed, followed by an approach that transports this one rivulet path over the side window [12]. Most recently [13], those two methods were combined into one simulation where the method of resolving the surface water film is based on a Discrete Phase Film Model (DPFM). The DPFM family of models originate from the work of O'Rourke and Amsden [14]. This base model does not account for the effects of surface tension and partial wetting. The lack of these forces acting on the particles at the moving contact line has a significant impact on the prediction of the rivulets patterns of the flow on the front side window. In this approach, the particles only follow the shear stress, which leads to a discrepancy between experiment and simulation [11]. This inaccuracy can skew the design of functional systems and lead to undesired effects like reduced visibility of the side mirror. As it is impossible to avoid water on the side window completely, it is necessary to develop an active means of removing the accumulated water from the side window, which can be facilitated through the simulation. To overcome some of the drawbacks of the standard DPFM models, Kruse [7] outlined outstanding issues in the

model and introduced model corrections to derive a viable particle-based vehicle soiling model. Kruse has shown that *to a good extent the simulation resembles the soiling pattern* on the side window in the wind tunnel test observations in the case of a disabled drainage system. However, this nature of the particle-based models reduces the predictability of pooling and its motion dynamics and influence on the primary phase. This requires an Eulerian model.

Naturally, the VOF method of Hirt [15] comes to mind. However, in spite of increased accuracy this approach is still constrained by computational costs that come from the requirements on the computational grid associated with explicitly resolving the wall film velocity profile and capturing the interface curvature. Thus, since the pioneering work of Karbon and Longman [8], a Continuous Phase Film Model (CPFM) that follows the work of Bai Gosman [16] and Foucart [17] can be considered a very good candidate to present results allowing for a satisfactory and accurate qualitative and quantitative analysis as shown in [18] and [19].

The Bai Gosman model was adopted by Meredith [20] to be used in fire suppressants [21]. Within iconCFD, this model is implemented and improved so it can further advance the understanding of exterior water management.

A very similar approach has been recently utilized in a study focusing on the prediction of the water ingress into the septum of an air intake [22], in which the outcomes of two implemented dispersed multiphase (DMP) models are compared. It has shown the potential of this modeling approach to correctly capture the complete description of water dynamics over the vehicle surface in rainy conditions.

## 5 Virtual Representation

The environment in a climatic wind tunnel has been represented virtually. Rain consists of a mixture of water droplets and air. In the context of the multiphase analysis that has been conducted, the air is denoted as the primary phase and the rain droplets are called the Lagrangian phase due to the methods applied for their resolution. The water film is called the secondary phase.

A precise resolution of the primary airflow is key to accurately predict the water behavior on the vehicle surface. Within this study, the primary phase is resolved with the WLTP-certified high fidelity transient external aerodynamics methodology that is employed at SKODA AUTO and uses the transient CFD solver.

Due to the temperature requirements for climatic testing (-40 to 60 $^{o}$C) the volume of the air in the testing section of a climatic wind tunnel is effectively smaller than that of a standard aerodynamic wind tunnel. It was anticipated that the Climatic Wind Tunnel layout dimensions might influence the results and, hence, prior to the measurement of the A-pillar overflow, a controlled experiment of pressure traces at various locations on the vehicle surface has been carried out by the authors using p-strips [23], a measurement tool based on MEMS digital absolute pressure sensors. This enabled a quick and un-intrusive measurement of pressure on the body.

The outcomes of this verification, illustrated in Figure 3, evince the necessity to adopt a DES-based ( [24], [25]) approach to model the airflow to correctly capture the

intrinsic structures near the A-pillar. However, as the ultimate aim of the study is to evaluate the on-road conditions, the reduction of the size domain has been neglected.

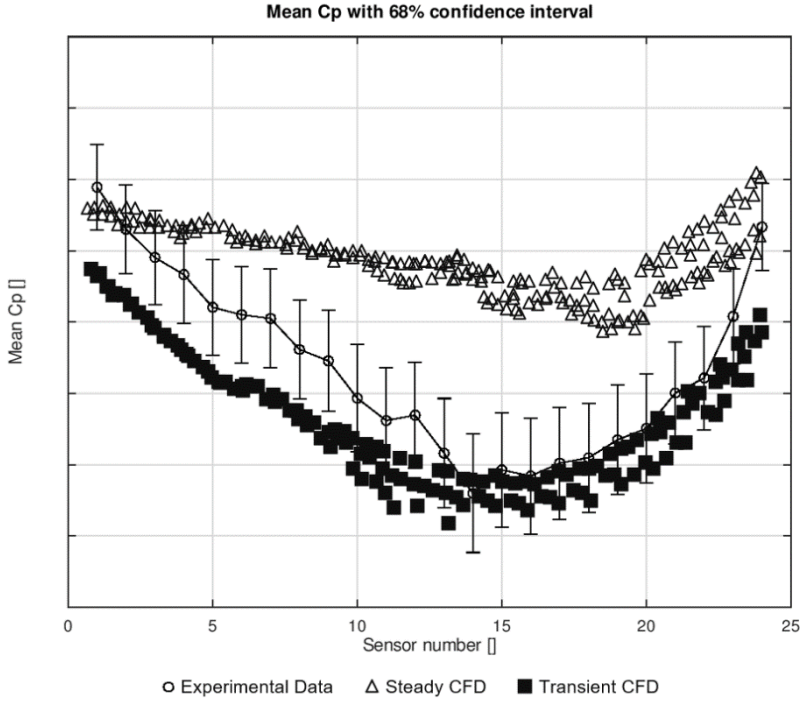


**Fig. 3.** Comparison of Experimental (MEMS), Steady CFD (RANS) and Transient CFD (DES) data evaluated in the middle of the A-pillar

### 5.1 Film Model Approach

One can arrive at the presented thin-film model through various paths. The most common are:

- Bai Gosman developed the model from jump conditions [26].
- Through the leading term analysis of the Navier Stokes equations, exploiting the small aspect ratio between the film thickness $\delta_f$ and the characteristic length scales of a vehicle body [27].
- Identifying the film equations as a special limit of the shallow water equations [28] with a specific velocity profile and source terms.

Here, the last approach is taken to highlight the main ideas behind the model derivation and to guide the understanding of the concepts specific to this methodology. The starting point is the Navier Stokes equations. In order to reduce the computational time, a quadratic velocity profile in the wall-normal direction can be considered. Assuming

the x-y direction to be tangential to a surface of the vehicle body and z to be the normal direction, the velocity u has the form of:

$$\boldsymbol{u}(\boldsymbol{x},\boldsymbol{y},\boldsymbol{z}) = \mathbf{3}\cdot\boldsymbol{u_f}(\boldsymbol{x},\boldsymbol{y})\left(\frac{\boldsymbol{z}}{\boldsymbol{\delta_f}(\boldsymbol{x},\boldsymbol{y})} - \frac{\boldsymbol{z^2}}{\mathbf{2}\cdot\boldsymbol{\delta_f^2}(\boldsymbol{x},\boldsymbol{y})}\right) \tag{1}$$

In the case of a constant film density $\rho_f$, the film velocity $\boldsymbol{u_f}$ is taken as a depth average of the actual velocity u over the film thickness $\delta_f$

$$\delta_f \boldsymbol{u_f} = \int_{\mathbf{0}}^{\boldsymbol{\delta_f}} \boldsymbol{u}\,\mathrm{d}z \quad \text{and} \quad \boldsymbol{u}(x,y,z) = \boldsymbol{u}_f(x,y) + \acute{\boldsymbol{u}}(x,y,z) \tag{2}$$

and the velocity can be decomposed into a mean part and a deviation from the mean $\acute{\boldsymbol{u}}$. This offers a significant computational time saving, since in the normal direction, only one layer of cells is needed to resolve the film motion, and only two equations need to be solved

$$\partial_t \rho_f \delta_f + \partial_{x_j} \rho_f \delta_f u_{f,i} = \gamma_{\delta_\mathrm{f}} \tag{3}$$

$$\partial_t \rho_f \delta_f u_{f,i} + \partial_{x_j} \rho_f \delta_f u_{f,i} u_{f,j} = -\delta_f \partial_{x_i} p + \gamma_{u_{f,i}} \tag{4}$$

What is essentially challenging in this model is the interaction of the various source terms ($\gamma_{\delta_f}, p, \gamma_{u_{f,i}}$) in the balance equations, which are related to the complex physics of various mechanisms of water film motion. Conservation of mass, which is represented by the first balance equation (3), effectively means that the film thickness can change only through inflow/outflow or by mass addition $\gamma_{\delta_f}$. On the other hand, the momentum equation can be viewed as representing film motion resulting from the balance of normal forces acting on the film understood through the pressure p and the various forces acting in the film tangential direction.

The pressure term $p$ contains terms associated with the influence of hydrostatic pressure ($\rho g_n \delta_f$), capillary pressure through surface tension $\sigma$ [29], the pressure imposed by the primary phase $p_g$ and the normal component of the momentum $p_l$ inflicted by impinging droplets

$$p = -\rho g_n \delta_f - \sigma \partial_{x_i} \partial_{x_i} \delta_f + p_g + p_l \tag{5}$$

The tangential source term $\boldsymbol{\gamma_{u_f}}$ comprise the effects of partial $\boldsymbol{f}_\theta$ wetting, the tangential portion of the gravitation body force, the tangential momentum transfer from impinging droplets $\boldsymbol{f}_l$, the simplified model of the diffusion with film viscosity $\mu_f$ and the force imposed by the wipers $\boldsymbol{f}_w$

$$\boldsymbol{\gamma_{u_f}} = \boldsymbol{f}_\theta + \rho_f \delta_f \boldsymbol{g}_t + \boldsymbol{f}_l + \mu_f \Delta \boldsymbol{u} + \boldsymbol{f}_w \tag{6}$$

The other source terms often associated with CPFM models in internal combustion engine applications [16] can be neglected. A more detailed description of the considered source terms is provided in the following subsections.

**Momentum Diffusion Modeling.** Within the laminar thin-film limit, it is possible to save computational effort, and instead of directly solving for the depth-averaged Laplacian term, the effects of momentum diffusion can be modeled through a suitable water film to the wall $\boldsymbol{\tau}_w^f$ and air to water film $\boldsymbol{\tau}_f^a$ shear stress selections.

$$\mu_f \Delta \boldsymbol{u} \approx \boldsymbol{\tau}_f^a + \boldsymbol{\tau}_w^f \tag{7}$$

The term $\boldsymbol{\tau}_w^f$ can be accounted for through a Navier-slip condition,

$$\boldsymbol{\tau}_w^f \approx 3 \cdot \mu \cdot \frac{\boldsymbol{u}_f^{rel}}{\delta_f}. \tag{8}$$

This condition is consistent with the selected velocity profile and has been experimentally verified to represent valid water film flow in the laminar limit [30]. As $\boldsymbol{\tau}_f^a$ is usually much lower in magnitude than $\boldsymbol{\tau}_w^f$, a simplified model of

$$\boldsymbol{\tau_a^f} \approx C_f \rho_{air} \left|\boldsymbol{u}_f^{rel}\right| \boldsymbol{u}_f^{rel} \tag{9}$$

can be adopted to sufficient accuracy in cases where the direct calculation of $\boldsymbol{\tau}_a^f$ from the primary flow is not available, as further commented in the Coupling Methods and their Application section.

**Partial Wetting**. In the given limit of a thin film, it is possible to consider two approaches to modeling the effects of the movement of the film in the close vicinity of the contact line that separates the wet and dry surfaces. It is possible to either assume a no-slip condition for the film and model the motion through a non-Newtonian, shear-thinning Cauchy stress response [31] or to take a more pragmatic approach and prescribe a certain slip through a force term that incorporates the effects of the contact angle $\theta$ and the movement of the contact line. This latter approach has been selected in this study.

*Contact Angle Force.* The equilibrium contact angle $\theta_e$ characterizes the wettability of a surface by a liquid. For $\theta_e < 90°$ the liquid displays hydrophilic behavior, while for $\theta_e > 90°$, the wetting is hydrophobic in nature. To model this phenomena, Young's law is applied together with the balance of interfacial forces at the front of the film [32] can be considered

$$\boldsymbol{f}_\theta = C_\theta \sigma (1 - cos\,\theta) + \boldsymbol{f}_{cl} \tag{10}$$

This enables the force to be quantified through both

- the correlation parameter $C_\theta$
- the physical variables of the contact angle $\theta$ and the surface tension $\sigma$.

$\theta_e$ provides an accurate representation for the case of static or quasi-static water film flows. In a vehicle application, the movement of the water film is dynamic and hysteresis, a difference between the advancing $\theta_a$ and receding $\theta_r$ contact angle is observed.

This is effectively modeled by resolving the contact line movement through an equivalent source term $\boldsymbol{f}_{cl}$ that acts against the motion of the contact line creating a hysteresis.

*Contact Line Movement*. The notion of a precursor film thickness $\delta_{crit}$ model is often recommended ( [27], [29], [20], [33]) and is adopted here to represent the force necessary to displace the contact line $\boldsymbol{f}_{cl}$. It assumes that for a water film with an equilibrium contact angle $\theta_e$, the contact line can be displaced only if $\delta_f > \delta_{crit}$ and

$$\boldsymbol{f}_{cl} = -\frac{\boldsymbol{u}_f}{\delta_{crit}}, \tag{11}$$

This approach, however, evinces an insufficient rivulet to droplets transition [20]. To alleviate this inaccuracy, a $\theta$ contact angle as a function of the film velocity close to the interface has been selected in iconCFD with model inputs aligned with the contact angle observed in car paints, windows and sealant rubbers [34].

**Wiper Model**. In the past, various means of representing the windscreen wiper have been applied. Most notably,

- In their original study, Karbon and Longman [8] utilized a periodic surface water source to distribute the water on the windshield.
- Foucart and Blain [9] represented the periodic force acting on the water film on the windshield surface through a swept virtual plane.
- In [13] wiper effects were represented through a line force applied to the DPFM representation of the film. In their follow-up study, they synchronized the wiper motion with a primary phase simulation in which the influence of wipers on the primary flow had been included through an immersed boundary method (IBM) method [35], where the effects of water film surface tension were neglected.
- Most recently [22] a mesh overset method was used for the wiper.

An overset method avoids remeshing at each timestep and can capture wiper blade deformation. However, similar to a VOF method, it comes at the expense of increased computational time [36], which in turn could require a coarsened [22] computational mesh for the water film management simulation. The present study adopts the external aerodynamics mesh directly and seamlessly creates the film region mesh from it. As a consequence, the wiper model, recently implemented in iconCFD, follows the work of Pinelli [1] and introduces the wiper source term $\boldsymbol{f}_w$ through an application of the IBM with an efficient wiper blade position search algorithm that does not significantly increase the computational time of the simulation.

## 5.2 Rain Representation

The Lagrangian-Eulerian (LE) approach is suitable for representing the dispersed multiphase flow of rain in air. Herein the rain droplets are represented in a Lagrangian reference frame, while the primary phase flow field is resolved in the Eulerian frame.

The communication between the two phases happens in a segregated manner through source terms. The droplet motion is governed by Newton's second law

$$m_d \cdot \frac{dv_d}{dt} = \sum \boldsymbol{F}_a \tag{12}$$

where the sum of acting forces $\boldsymbol{F}_a$ models the interaction with the primary phase. In the case of a water management simulation focused on side-window visibility, it is sufficient to account only for

- Spherical droplet drag through Liu's dynamic drag coefficient [37]
- Virtual mass to account for the difference in droplet and primary phase accelerations
- Gravity (since a typical droplet diameter in the rain varies from micro-meters up to several millimeters [38])
- The influence of the primary phase pressure gradient on the droplets

Other, higher-fidelity droplet models (e.g. secondary breakup [39], turbulence dispersion [40], inter-droplet collisions and coalescence [41]) are also available in iconCFD. However, to represent the rain characteristics observed in the experiment, it is possible to neglect them and still achieve a qualitative match with the rain deposition behavior on the vehicle surface.

**Rain Deposition.** The action of droplet impact causes a point of mass $\gamma_{\delta_f}$ and momentum $p_l$ and $\boldsymbol{f}_l$ to transition from a Lagrangian phase to water film. The physics of water droplet impact depends on the condition of the surface and the properties of the droplet and can be suitably characterized by Weber's impact number

$$We_d = \frac{\rho_d |u_d^{\perp}|^2 d}{\sigma_d} \tag{13}$$

for droplets of diameter d.

For the droplets observed in the experiment, the well-known Bai model [16] is a well-established and utilized interaction treatment that can distinguish droplet adhesion, rebound, spreading or splash, based on user specifications.

**Droplet Re-Entrainment.** Due to the balance of forces on the surface of the water film, droplet separation from the water film can occur. Predominantly, it can be induced by the interaction of the water film with the air, by a sudden change in geometry or through dripping. These phenomena are often closely intertwined, and it is difficult to make a clear-cut separation between them. This has motivated the recent rise in a detailed hybrid VOF application to handle such situations, e.g. [42] [43].

However, since the major focus of this study is the A-pillar overflow, this secondary detachment is neglected in this study.

**Coupling Methods and their Application.** In the practice of vehicle water management that is outlined in the introduction, it is assumed that the droplets have a negligible effect on the primary phase, and, thus, only the primary flow affects the droplets without any feedback from the droplets on the primary flow. Therefore, it is possible to freeze the flow and solve only for the droplet and water film motion. This is the so-

called **one-way** coupling that serves as a time-efficient means of simulation and is adopted in this study.

For flows with a high Stokes number *St* (ratio of the response time of the dispersed to the continuous phase, e.g. [44]) and for higher particle diameters in zones with higher droplet concentrations, the feedback cannot be neglected. In the case of the A-pillar overflow, it is sufficient to adopt one-way coupling. However, to observe the water film behavior e.g. on the mirror glass of the side-view mirror, two-way coupling, where the primary phase momentum is influenced by the Lagrangian phase, is important to predict correct deposition of the droplets stripped from the side mirror body on the side window, a technique that is commonly used in self-soiling simulations [45].

# 6 Results

To predict the characteristics of the A-pillar over-flow, the experimental setup is recreated virtually. The spray rack geometry is simplified by a random box injector placed ahead of the vehicle body as highlighted in Fig. 4. The rain particles are modeled by droplets with a diameter within the range of 0.2 to 2 mm. Three different vehicle speeds, 90, 110 and 130 kph, are considered. The wiper speed is such that one complete motion occurs every 2 seconds.

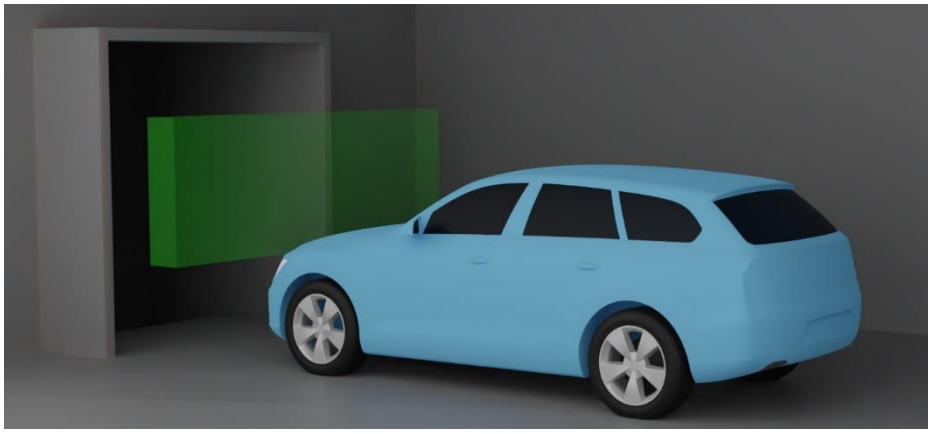

**Fig. 4.** Schematics of the box used to inject rain droplets relative to the vehicle position (AeroSUV Estate used for this demonstration [46])

## 6.1 Windscreen Wiper Effects

Fig. 5 depicts the behavior of water in the vicinity of the wiper. It can be seen that water agglomeration into water streaks is present both in the experiment and the simulation.

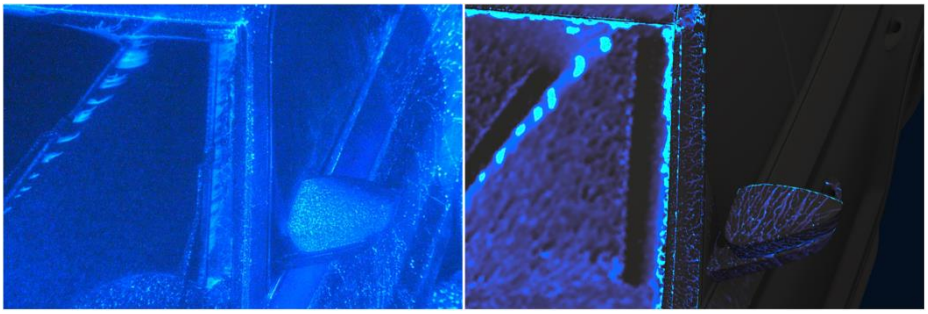

**Fig. 5.** A comparison of water film behavior close to a wiper blade (90 kph, windscreen wipers close to the upstroke position) between experimental (left) and simulation (right) data

One can further observe, from Fig. 5, that for short simulation and experimental physical times the wiper motion does not push the water over the A-pillar. Once more water is accumulated, wiper-induced over-flow can be observed (Figure 6). In the wind tunnel testing, a strong wiper pull-back can be also seen near the A-pillar. This is caused by the intricate interaction of the airflow with the wiper in the close vicinity of the A-pillar. In the present study, the airflow is kept frozen during the simulation. Thus, the wiper pull-back effect is not captured. This creates a slight discrepancy between simulation and reality which is the subject of a separate study. However, on the studied vehicle this does not significantly affect the A-pillar overflow.

The difference in the amount of water present on the side window at those similar wiper events in Fig. 6 is because the wiper motion in experiment has not been synchronized with the start of the spray and the relative offset of wiper activation varies at different vehicle speeds.

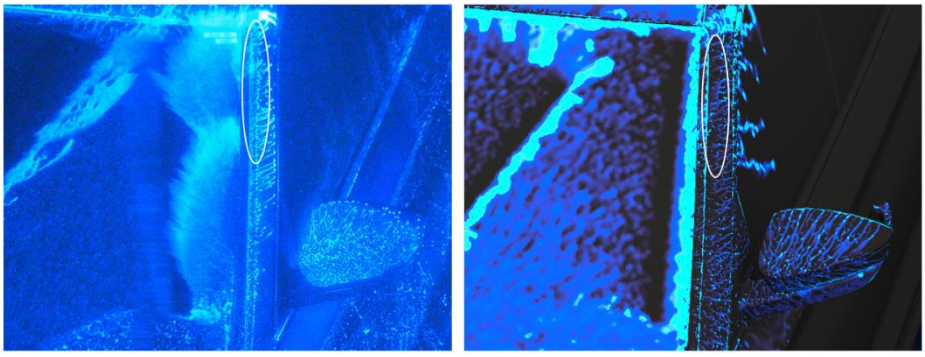

**Fig. 6.** A comparison of wiper induced A-pillar overflow (90 kph, windscreen wipers close to the upstroke position) between experimental (left) and simulation (right) data

### 6.2 Film Behavior on Side Window

The initial point of the film overflow is accurately predicted for the 90 kph load case (Fig. 7).

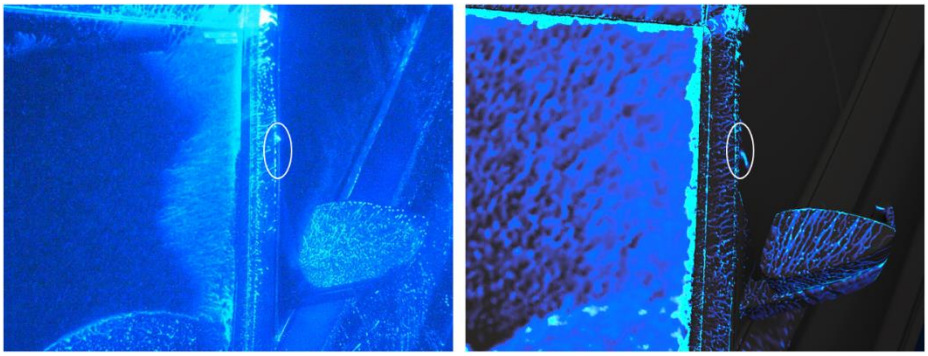

**Fig. 7.** A comparison of the initial location of A-pillar overflow (90 kph, windscreen wipers close to the upstroke position) between experimental (left) and simulation (right) data

Unfortunately, for the remaining vehicle speeds, the data acquisition had started after the water film breached the A-pillar. The identification of the first breach point and other instances of water creating a rivulet between the door frame and the side window is key to predict the behavior on the side window (see Fig. 8). Once such rivulet is formed, the water film follows this path unless disturbed (see Partial Wetting paragraph in section 5.1) by air fluctuations. However, in the present methodology, the primary flow field is kept frozen over time to allow for short turnaround times and relatively long physical time simulated (10 seconds) in which the simulation reaches a quasi-steady state. This resolution is directly affected by the full history of the film movement, hence the importance of correct prediction of the A-pillar overflow locations on the qualitative behavior of the water film on the side window.

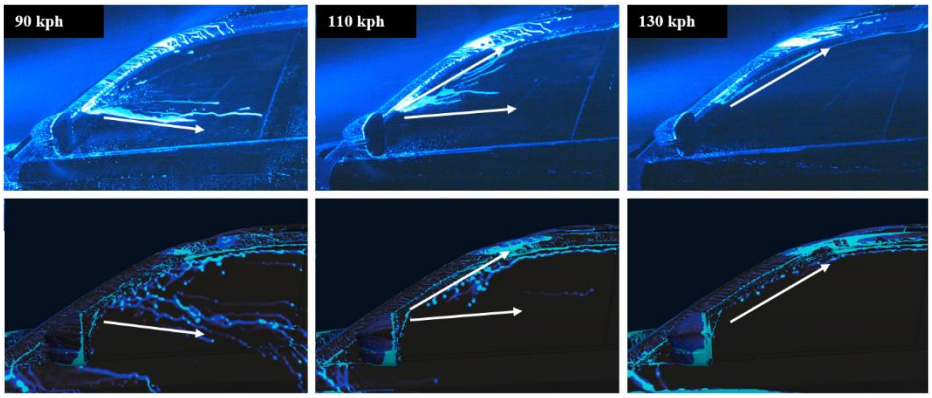


**Fig. 8.** Comparison of experimental data (top) and simulation data (bottom) predictions for the water film behavior on the side window at 10s of physical time

As shown in Fig. 8, the water film development over the front side window is qualitatively well captured. Quantitatively, it must be noted that in the experiment the main overflow of the A-pillar occurs at a lower location than in the simulation. This discrep-

ancy is caused by the geometrical simplification of the groove-shaped door rubber sealing. This V-shaped rubber sealing is omitted in the external aerodynamics simulation following the best practice. However, the experiment shows this groove can transport the water from the top section of the A-pillar towards the observed overflow location and its geometry should be taken into consideration in further EWM studies.

## 7 Summary

The presented methodology gives a good agreement with the experimental data for the prediction of A-pillar over-flow.

The effect of the windscreen wipers is modeled accurately and the lack of the modeled wiper pull-back does not negatively influence the qualitative representation of the results on the side window. The simulation predicts accurately both the point of first over-flow of the A-pillar and the water film behavior on the side window.

This is a combination of the higher fidelity air-flow model and the implementation of the presented implementation of CPFM model and its linkage to the Lagrangian representation of the rain droplets

A more detailed depiction of the experimental rain source and a more detailed description of the areas of interest has the potential to further mitigate the observed differences in the amount of water deposited on the A-Pillar and side window and is currently being evaluated.

## Acknowledgments

The authors are grateful to SKODA AUTO for granting permission for the publication of this work. They would also like to thank Mr. Petr Simon and Mr. Tomas Hlava (SKODA) for the experimental data presented, along with Dr. Peter Ireland (ICON) for their helpful suggestions.

## References

1. A. Pinelli, I. Z. Naqavi, U. Piomelli and J. Favier, Immersed-boundary methods for general finite-difference and finite-volume Navier–Stokes solvers, Journal of Computational Physics, vol. 229, pp. 9073-9091, 2010.
2. Icon Technology And Process Consuting®, [Online]. Available: https://www.iconcfd.com.
3. T. Hagemeier, M. Hartmann and D. Thévenin, Practice of vehicle soiling investigations: A review, International Journal of Multiphase Flow - INT J MULTIPHASE FLOW, vol. 37, pp. 860-875, 10 2011.

4. M. Bannister, Drag and Dirt Deposition Mechanisms of External Rear View Mirrors and Techniques Used for Optimisation, in SAE Technical Paper, 2000.
5. A. Borg and R. Vevang, On the Development of a Wind Tunnel method for the Prediction of Exterior Contamination, in 5th MIRA International Conference on Vehicle Aerodynamics, UK, 2004.
6. T. Landwehr, T. Kuthada and J. Wiedemann, Methodical Investigation of Vehicle Side Glass Soiling Phenomena, in Progress in Vehicle Aerodynamics and Thermal Management, Cham, 2018.
7. N. Kruse and K.-H. Chen, Exterior Water Management Using a Custom Euler-Lagrange Simulation Approach, in SAE World Congress & Exhibition, 2007.
8. K. J. Karbon and S. E. Longman, Automobile Exterior Water Flow Analysis Using CFD and Wind Tunnel Visualization, in International Congress & Exposition, 1998.
9. H. Foucart and E. Blain, Water-flow Simulation on Vehicle Panels by Taking into Account the Calculated Aerodynamic Field, in 2005 SAE Commercial Vehicle Engineering Conference, 2005.
10. A. P. Gaylard, K. Kirwan and D. A. Lockerby, Surface contamination of cars: A review, Proceedings of the Institution of Mechanical Engineers, Part D: Journal of Automobile Engineering, vol. 231, pp. 1160-1176, 2017.
11. A. P. Gaylard, M. Fagg, M. Bannister, B. Duncan, J. I. Gargoloff and J. Jilesen, Modelling A-Pillar Water Overflow: Developing CFD and Experimental Methods, 2012.
12. J. Jilesen, A. Gaylard, I. Spruss, T. Kuthada and J. Wiedemann, Advances in Modelling A-Pillar Water Overflow, in SAE 2015 World Congress & Exhibition, 2015.
13. J. Jilesen, A. Gaylard, T. Linden and A. Alajbegovic, Update on A-Pillar Overflow Simulation, in WCX World Congress Experience, 2018.
14. P. J. O'Rourke and A. A. Amsden, A Particle Numerical Model for Wall Film Dynamics in Port-Injected Engines, in 1996 SAE International Fall Fuels and Lubricants Meeting and Exhibition, 1996.
15. C. W. Hirt and B. D. Nichols, Volume of fluid (VOF) method for the dynamics of free boundaries, Journal of Computational Physics, vol. 39, pp. 201-225, 1981.
16. C. Bai and A. D. Gosman, Mathematical Modelling of Wall Films Formed by Impinging Sprays, in International Congress & Exposition, 1996.
17. H. Foucart, C. Habchi, J. F. Le Coz and T. Baritaud, Development of a Three Dimensional Model of Wall Fuel Liquid Film for Internal Combustion Engines, in International Congress & Exposition, 1998.
18. F. Campos, F. Mendonca, S. Weston and M. Islam, Vehicle soiling simulation, in 6th MIRA International Vehicle Aerodynamics Conference, 2006.
19. F. Campos, F. Mendonca, S. Weston and M. Islam, CFD simulation of vehicle soiling, in NAFEMS World Congress, 2007.
20. K. Meredith, J. Vries and Y. Xin, A numerical model for partially-wetted flow of thin liquid films, 2011.
21. K. Meredith, J. Vries, Y. Wang and Y. Xin, A comprehensive model for simulating the interaction of water with solid surfaces in fire suppression environments, Proceedings of the Combustion Institute, vol. 34, pp. 2719-2726, 2013.

22. G. Lombardi, A. Ercoli, M. Maganzi and G. Angeli, Comparison of two Multiphase Procedures on a Commercial Vehicle in Rain Conditions, International Journal of Automotive Technology, vol. 20, pp. 1123-1129, 01 12 2019.
23. F. Wittmeier, T. Kuthada, J. Filipsky and J. Cizek, New MEMS Pressure Sensors for Transient Aerodynamic Measurements, ATZ worldwide, vol. 120, pp. 38-41, 4 2018.
24. T. Han, S. Kaushik, K. Karbon, B. Leroy, K. Mooney, S. Petropoulou and J. Papper, Adjoint-Driven Aerodynamic Shape Optimization Based on a Combination of Steady State and Transient Flow Solutions, 2016.
25. R. Lietz, L. Larson, P. Bachant, J. Goldstein, R. Silveira, M. Shademan, P. Ireland and K. Mooney, An Extensive Validation of an Open Source Based Solution for Automobile External Aerodynamics, in WCX™ 17: SAE World Congress Experience, 2017.
26. J. M. Delhaye, Jump conditions and entropy sources in two-phase systems. Local instant formulation, International Journal of Multiphase Flow, vol. 1, pp. 395-409, 1974.
27. S. O'Brien and L. Schwartz, Theory and modeling of thin film flows, Encyclopedia of Surface and Colloid Science, pp. 5283-5297, 1 2002.
28. L. D. Landau and E. M. Lifshitz, Fluid Mechanics - Landau and Lifshitz: Course of Theoretical Physics, 2. Aufl. ed., Amsterdam: Elsevier, 2013.
29. J. Diez and L. Kondic, Computing Three-Dimensional Thin Film Flows Including Contact Lines, Journal of Computational Physics, vol. 183, pp. 274-306, 11 2002.
30. M. Trela, A semi-theoretical model of stability of vertical falling liquid films, Chemical Engineering Science, vol. 49, pp. 1007-1013, 1994.
31. D. E. Weidner and L. W. Schwartz, Contact-line motion of shear-thinning liquids, Physics of Fluids, vol. 6, pp. 3535-3538, 1994.
32. P.-G. De Gennes, Wetting: statics and dynamics, Reviews of modern physics, vol. 57, p. 827, 1985.
33. S. F. Kistler, Hydrodynamics of wetting, Wettability, vol. 6, pp. 311-430, 1993.
34. I. Spruß, Ein Beitrag zur Untersuchung der Kraftfahrzeugverschmutzung in Experiment und Simulation, Springer, 2016.
35. J. Jilesen, A. Gaylard and T. Linden, Numerical Investigation of Wiper Drawback, in SAE Technical Paper, 2019.
36. D. Chandar, B. Boppana and V. Kumar, A Comparative Study of Different Overset Grid Solvers Between OpenFOAM, StarCCM+ and Ansys-Fluent, 2018.
37. A. B. Liu, D. Mather and R. D. Reitz, Modeling the Effects of Drop Drag and Breakup on Fuel Sprays, in SAE Technical Paper, 1993.
38. M. Aoki, H. Iwai, K. Nakagawa, S. Ishii and K. Mizutani, Measurements of rainfall velocity and raindrop size distribution using coherent Doppler lidar, Journal of Atmospheric and Oceanic Technology, vol. 33, pp. 1949-1966, 2016.
39. R. Reitz, Modeling atomization processes in high-pressure vaporizing sprays, Atomisation Spray Technology, vol. 3, pp. 309-337, 1 1987.
40. A. D. Gosman and E. , Aspects of Computer Simulation of Liquid-Fueled Combustors, Journal of Energy, vol. 7, pp. 482-490, 1983.
41. P. J. O'Rourke, Collective drop effects on vaporizing liquid sprays, 11 1981.

42. T. Tivert, A. Borgy, J. Marimon and L. Davidson, Wind-driven rivulet over an edge with break-up, in Proceedings of the ICMF 2007, 6th International Conference on Multiphase Flow, 2007.
43. V. R. Shrimali, S. Rawat and R. K. Duggirala, A Methodology to Simulate Water Stripping Phenomenon in Vehicle Soiling: An Eulerian to Lagrangian Approach, Red, vol. 400, p. 24. , 2018
44. C. Crowe, J. Schwarzkopf, M. Sommerfeld and Y. Tsuji, Multiphase flows with droplets and particles, 2011.
45. A. P. Gaylard, J. Pitman, J. Jilesen, A. Gagliardi, B. Duncan, J. Wanderer and A. Konstantinov, Insights into Rear Surface Contamination Using Simulation of Road Spray and Aerodynamics, SAE Int. J. Passeng. Cars - Mech. Syst., vol. 7, pp. 673-681, 4 2014.
46. C. Zhang, M. Tanneberger, T. Kuthada, F. Wittmeier, J. Wiedemann and J. Nies, Introduction of the AeroSUV-A New Generic SUV Model for Aerodynamic Research, in SAE Technical Paper, 2019.